BOLETIN DE LA SOCIEDAD ESPAÑOLA DE
Cerámica y Vidrio
www.elsevier.es/bsecv

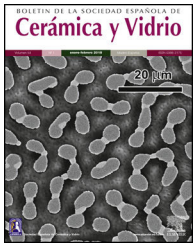

High temperature mechanical properties of polycrystalline Y_2SiO_5

Rafael Cabezas-Rodriguez[a], *Desirée Ciria*[a,b], *Julián Martinez-Fernandez*[a], *Guilhem Dezanneau*[b], *Fabienne Karolak*[b], *Joaquín Ramirez-Rico*[a,*]

[a] *Dpto. Física de la Materia Condensada and Instituto de Ciencia de Materiales de Sevilla, Universidad de Sevilla – CSIC, Avda. Reina Mercedes SN, 41012 Sevilla, Spain*
[b] *Laboratoire Structure, Propriétés et Modélisation des Solides, CentraleSupélec, Université Paris-Saclay, 3 Rue Joliot-Curie, 91190 Gif-sur-Yvette, France*

ARTICLE INFO

Article history:
Received 23 June 2021
Accepted 13 September 2021
Available online 23 October 2021

Keywords:
Yttrium orthosilicate
High temperature
Creep
Compression

ABSTRACT

The high temperature mechanical properties of polycrystalline Y_2SiO_5 were studied in compression at temperatures in the range of 1200–1400 °C, both in constant strain rate and constant stress experiments. To examine the effect of grain size on the plastic deformation, two routes were used for the synthesis and sintering of Y_2SiO_5: one of solid state reaction followed by conventional sintering in air, and one of sol–gel synthesis followed by spark-plasma sintering, resulting in starting grain sizes of 2.2 and 0.9 μm, respectively. Ceramics obtained by these routes exhibited different high-temperature compression behavior: while the conventionally processed ceramic exhibited grain growth during mechanical testing and a stress exponent close to one, compatible with diffusional creep, the spark-plasma sintered ceramic showed no grain growth but significant cavitation, a stress exponent close to two and partially superplastic behavior. These results have implications for the design and lifetime assessment of rare earth silicate-based environmental barrier coatings.

Propiedades mecánicas a alta temperatura del Y_2SiO_5 policristalino

Palabras clave:
Ortosilicato de itrio
Alta temperatura
Compresión
Fluencia

RESUMEN

Este trabajo aborda el comportamiento mecánico a compresión del Y_2SiO_5 policristalino a temperaturas entre 1200 °C y 1400 °C, tanto en experimentos de tensión constante como de velocidad de deformación constante. Para estudiar el efecto del tamaño de grano en la deformación plástica, se utilizaron dos rutas para la síntesis y sinterización de Y_2SiO_5: una de reacción en estado sólido seguida de sinterización convencional en aire, y una de síntesis sol-gel seguida de Spark-Plasma Sintering, obteniéndose tamaños de grano iniciales de 2,2 y 0,9 μm, respectivamente. Los policristales obtenidos por estas rutas mostraron distinto

* *Corresponding author.*
E-mail address: jrr@us.es (J. Ramirez-Rico).
https://doi.org/10.1016/j.bsecv.2021.09.008

comportamiento en compresión a alta temperatura: mientras que el cerámico convencionalmente exhibió crecimiento de grano y un exponente de tensión cercano a uno, compatible con un mecanismo de fluencia por difusión, el cerámico procesado por Spark-Plasma Sintering no mostró crecimiento de grano pero sí cavitación, un exponente de tensión cercano a 2 y un comportamiento parcialmente superplástico. Estos resultados tienen implicaciones para el diseño y la evaluación de la vida útil de recubrimientos de barrera ambiental a base de silicatos de tierras raras.

Introduction

Ceramic matrix composites (CMCs) and silicon-based ceramics (such as Si_3N_4, SiC) are promising candidates for high temperature structural applications such as next generation gas turbine engines since they exhibit low density, excellent high-temperature mechanical properties, and good thermomechanical stability [1,2]. In presence of oxygen from dry air environments, silicon-based ceramics form a protective silica scale, responsible for their excellent high temperature oxidation resistance at these conditions [3]. However, this SiO_2 layer is susceptible of attack by impurities such as alkali salts and is unstable in the presence of water vapor, resulting in rapid ceramic recession. Thus, Si-based ceramics present a lack of environmental durability [4–6].

Currently, environmental barrier coatings (EBCs) are being used to limit the volatilization and recession of the passivating oxide layer, extending the operating conditions of SiC based ceramics in combustion environments [7]. Rare earth silicates (such as yttrium silicates) are being explored as topcoats in third-generation EBCs [8–11] due to their low thermal expansion coefficient, thermochemical stability and higher temperature capability than current generation EBCs formed of mullite and barium-strontium aluminosilicates (BSAS) [12–14]. Yttrium silicates (e.g., yttrium orthosilicate, Y_2SiO_5) are promising materials for improving oxidation and erosion protection since they exhibit a high melting point, low volatilization rate, low thermal expansion coefficient, and low oxygen permeation constant [15,16]. There are several synthesis methods to obtain Y_2SiO_5 powders such as solid-state reaction, sol-gel, and hydrothermal methods [17–19]. Nevertheless, the preparation of single-phase fully dense Y_2SiO_5 bulk material by these methods presents several problems [20–22] such as presence of secondary undesired phases, significant porosity in bulk samples, etc.

Despite the interest in rare earth silicates as topcoats for EBCs, and while room temperature mechanical properties and thermal properties of Y_2SiO_5 polycrystalline materials have been studied in detail [22–24], little is known regarding their high-temperature mechanical properties and, to the authors' knowledge, no data on the creep behavior of these materials has been published. In EBC multilayers, the topcoat is subjected to stresses that arise from the thermal expansion mismatch between the different layers that form the coating, which can vary from tensile to compressive as the EBC is thermally cycled during operation [25] and can be affected by reaction with molten glass deposit within engines [26]. Thus, it is necessary to understand Y_2SiO_5 behavior at high temperatures to evaluate its performance and lifetime for structural components and coatings for high temperature applications.

The aim of this work is then to study the mechanical properties of Y_2SiO_5 at temperatures that are relevant for their actual applications as elements of EBCs. To this end, we prepared Y_2SiO_5 ceramics via two different routes with the goal of obtaining ceramics with different microstructures. Then, the obtained ceramics were tested at temperatures in the range 1200–1350 °C in compression to determine their high-temperature plasticity and creep behavior. The change of creep behavior is discussed as a function of preparation route and grain size.

Experimental methods

Synthesis and sintering of Y_2SiO_5 ceramics

Two processing routes for Y_2SiO_5 were used in this work with the aim of obtaining ceramics with different grain sizes: solid state reaction followed by conventional sintering and sol–gel synthesis followed by spark-plasma sintering (SPS). The former process is expected to result in polycrystals with a larger grain size compared to the later one.

For conventional sintering, Precursor powders of Y_2O_3 (Sigma–Aldrich, 99.99%) and amorphous SiO_2 (Sigma–Aldrich, 99.95%) were mixed in stoichiometric ratios (1:1 molar) in isopropyl alcohol. To this mixture 3% mol. $LiYO_2$ was added as a sintering additive [20,27] and the resulting powder was milled in a planetary mill for 10 h and then calcined at 1500 °C for 2 h in air. The resulting powders were ball-milled again for 10 h to break all agglomerates and to achieve a homogeneous particle size. These powders were uniaxially pressed in a 13 mm diameter steel die at 100 MPa and then isostatically cold pressed at 200 MPa to form a green-body compact (density ~65–70%) that was subsequently sintered in a furnace at 1500 °C in air for 6 h.

For the second processing route, methods were adapted from a previous publication on $La_{9.33}Si_6O_{26}$ [28]. For the synthesis, commercially available reagents yttrium acetate $Y(CH_3COO)_3{\cdot}H_2O$ (Alfa Aesar, 99,9%) and tetraethoxysilane $Si(OC_2H_5)_4$ (TEOS, Alfa Aesar 99,9%) were used as precursors of Y^{3+} and Si^{4+} cations. Firstly, two solutions were prepared: one with ~16–17 g of yttrium acetate completely dissolved into ultra-pure water, and another containing ~6.7 mL silicon alkoxide, ~27 mL acetic acid and a small quantity of ultra-pure water. Acetic acid was used as double agent since it catalyzes

and controls the hydrolysis reaction of TEOS. Then, the second solution was poured into the first one and mixed thoroughly. The total volume of the solution obtained was 600 mL, with a pH value close to 3.8. After that, strong stirring was carried out for 2 h to obtain a clear transparent solution. This solution was sprayed into a liquid nitrogen bath to form frozen droplets that were transferred to a freeze-dryer in as short a time as possible to avoid melting. Freeze-drying was carried out in a Christ Alpha 2–4 LSC apparatus for 72 h under vacuum (1 Pa), with the condenser temperature fixed at −80 °C. Once this process was completed, the resulting white porous powder was calcined in air at 1400 °C for 4 h.

These powders were sintered using SPS to achieve fully dense materials using a graphite die 20 mm in diameter in a Dr. Sinter 2080 SPS furnace (Plateforme Fritage Flash, Thiais, France). The applied pressure was 100 MPa and the temperature was increased to 600 °C at a rate of 200 °C min^{-1} and then to 1200 °C at a rate of 50 °C min^{-1}. This temperature was held for 3 min before releasing the applied pressure and heating power. Natural cooling took around 10 min; thus, the entire process was undergone in less than one hour. Finally, the sintered ceramics were heated at 800 °C for 24 h in air to remove residual carbon coming from the graphite die.

Characterization

Density of the sintered ceramics was determined using a He-Pycnometer (Quantachrome Ultrapyc 1200e). Relative density was calculated from the theoretical density of Y_2SiO_5 (4.44 g cm^{-3}) and under the hypothesis that the synthesis reaction was complete and thus the whole sintered pellet contains only Y_2SiO_5.

Samples both as-fabricated and after mechanical testing were observed using a scanning electron microscope (SEM, FEI Teneo) and a transmission electron microscope (TEM, FEI Talos). For SEM observations samples were cut using a diamond coated wafering blade and polished by conventional metallographic methods using diamond abrasives down to 1 μm. To enhance the grain boundary contrast and facilitate the determination of grain size, samples were further thermally etched in air at 1300 °C for one hour. Grain size was determined using the linear intercept method. For TEM observation samples were cut into 3 mm disks and thinned abrasively down to 100 μm before dimpling and ion polishing.

The identification of crystalline phases in the sintered Y_2SiO_5 ceramics was performed using X-ray diffraction (XRD, D8 Advance 24, Bruker). Each pattern was measured at following conditions: Bragg-Brentano configuration θ–2θ using $Cu_{k\alpha}$ wavelength ($\lambda = 1.5418$ Å) filtered with a nickel foil in a XRD tube at voltage 40 kV and current intensity of 30 mA. Data acquisition was by means of continuous angular scanning in the 2θ region between 10° and 90° with a 0.03° step in 2θ. The resulting diffractograms were analyzed by the Rietveld method. Starting crystal structures were obtained from the PDF-4+2019 crystallographic database (International Centre for Diffraction data) for Y_2SiO_5 (PDF 00-036-1476) and Y_2O_3 (PDF 00-041-1105). The Fundamental Parameters approach was used to model instrumental peak broadening and the following parameters were refined: lattice parameters, sample displacement, Lorentzian broadening due to crystallite size, a 5-order Chebyshev polynomial to describe the background and a global scaling constant.

Mechanical testing

Samples were cut into parallelepipeds (3 mm × 3 mm × 5 mm) for mechanical testing and the load was applied in compression along the longest direction in all cases. Each sample's faces were ground plane-parallel using a diamond grinding wheel. Two types of experiments were performed: constant strain rate and constant stress.

Constant strain rate experiments were performed in an electromechanical Universal Testing Machine (Microtest EM1/50/FR) with an attached furnace. Load was applied using two 25.4 mm diameter alumina rods. Starting strain rate was in all cases 3.2×10^{-6} s^{-1} (the lowest attainable rate in our system) and the load was monitored using either a 1 kN or 5 kN rated load cell, depending on the temperature and load range. The tested temperatures were in the range of 1200–1350 °C. Samples were subjected to a small contact load that was maintained during heating at 10 °C/min until the final temperature, which was held for 1 h before the start of each test to allow for thermal stabilization of the system.

Constant stress (creep) experiments were carried out using a dead-weight machine (Microtest M/SCM-2-FP) in which the load is applied using a lever connected to the upper loading rod, while the lower rod is displaced to ensure constant stress. Sample contraction during the experiments was monitored using a linear variable displacement transducer outside the hot zone of the furnace, attached to the machine's frame. Strain and strain rates were determined from the instantaneous length $l(t)$ of the sample using:

$$\varepsilon(t) = \ln \frac{l_0}{l(t)}, \quad \dot{\varepsilon}(t) = \frac{d\varepsilon}{dt} \approx -\frac{1}{l(t)} \frac{\Delta l}{\Delta t} \tag{1}$$

Applied stresses were in the range of 20–60 MPa and temperatures were in the range 1300–1400 °C. As in the case of constant strain-rate experiments, samples were subjected to a small contact load that was maintained during heating, which was carried out at 10 °C/min until the final temperature. A soaking time of 1 h was allowed before the start of each.

Since the creep rate is a function of stress and temperature, but also of grain size, two types of experiments were performed. In constant temperature tests the applied stress was varied in 10 MPa discrete steps and the stress exponent for creep was calculated using the measured creep rates before and after the step. In constant stress experiments, the load was kept fixed, and the temperature was varied in 25 °C steps. This allowed us to calculate the activation energy for creep using the creep rates before and after the temperature change. The advantage of this differential method is that creep parameters are calculated at a 'constant microstructure', eliminating the influence of any grain growth that could be occurring during the experiments.

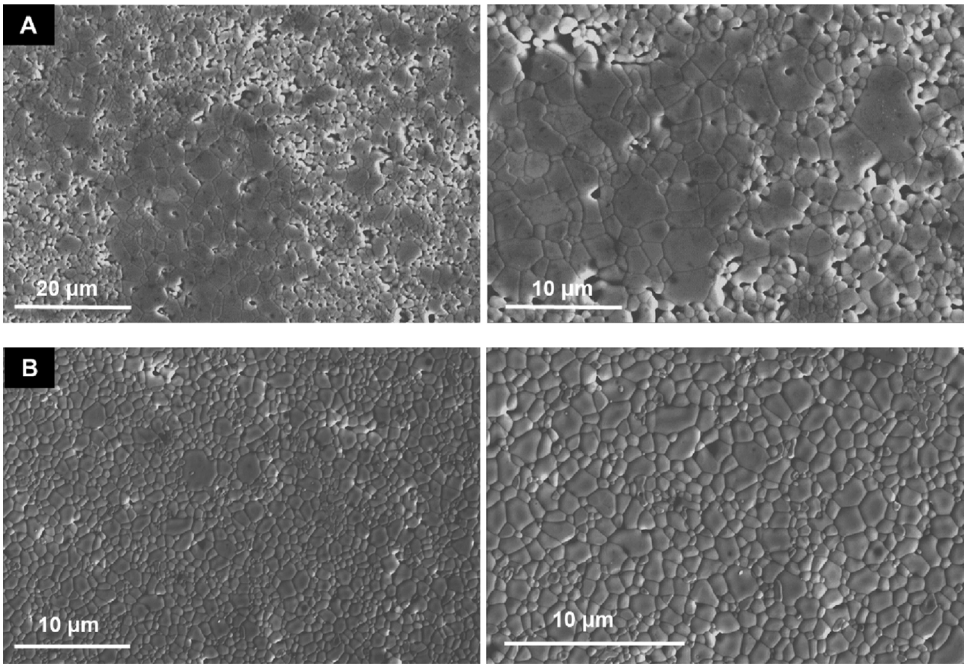

Fig. 1 – SEM micrographs of the sintered Y_2SiO_5 ceramics: (a) conventionally sintered Y_2SiO_5, (b) spark-plasma sintered Y_2SiO_5.

Table 1 – Absolute and relative density of the Y_2SiO_5 ceramics prepared in this work.

	Density ($\pm 0.01\,g\,cm^{-3}$)	Relative density ($\pm 1\%$)
Conventionally sintered	4.10	92
Spark-plasma sintered	4.22	95

Results and discussion

Microstructure and composition

The densities of the sintered Y_2SiO_5 ceramics are detailed in Table 1, while the microstructure is shown in Fig. 1. In the case of Y_2SiO_5 prepared by solid-state reaction and conventional sintering, grains are polygonal and equiaxed, with some visible porosity (panel a). The mean grain size was $2.2 \pm 1.2\,\mu m$. The spark-plasma sintered ceramic looks instead fully dense with no visible pores and shows a finer grain size of $0.9 \pm 0.4\,\mu m$ as determined by the linear intercept method.

XRD patterns of the sintered Y_2SiO_5 ceramics are shown in Fig. 2, along with the results of Rietveld refinement. In the case of conventionally sintered Y_2SiO_5, 5% wt. of unreacted Y_2O_3 was observed, apart from monoclinic Y_2SiO_5. For the spark-plasma sintered ceramics, only Y_2SiO_5 was detected, with no other phases present in the diffractogram. The presence of Y_2O_3 in the conventionally sintered ceramic is probably due to the addition of $LiYO_2$ as a sintering aid, which decomposes into Y_2O_3 and Li_2O at high temperatures, but also due to incomplete reaction of Y_2O_3 and SiO_2.

Constant strain rate tests

Fig. 3 shows the stress–strain curves for the Y_2SiO_5 ceramics at an initial strain rate of $3.2 \times 10^{-6}\,s^{-1}$ and temperatures from 1200 °C to 1400 °C for conventionally sintered polycrystals (panel a) and from 1200 °C to 1350 °C for spark-plasma sintered polycrystals (panel b). In the case of conventionally sintered Y_2SiO_5, the sample tested at 1200 °C exhibits catastrophic failure at a stress over 230 MPa after yielding, as the strain rate is too large to be accommodated via plastic deformation, resulting in the formation of microcracks that eventually coalesce resulting in the final fracture of the specimen. At 1250 °C a fragile-to-ductile transition is observed, and active plasticity mechanisms are sufficient to partially accommodate the externally applied deformation rate. This accommodation is however not enough to sustain homogeneous deformation and a continuous decrease in load is observed as deformation increases, eventually resulting in gracile failure. In contrast, at temperatures 1300 °C and higher, plastic deformation is sustained and high strains of ~10% and ~15% are observed, implying that at temperatures over 1300 °C plasticity mechanisms are active and able to accommodate deformation at the applied strain rate.

An examination of the microstructure of conventionally sintered Y_2SiO_5 ceramics after constant strain rate deformation reveals that significant grain growth took place during the tests, as can be seen in Fig. 4. The final mean grain size after the tests is included in Table 2.

In finer-grained, spark-plasma sintered Y_2SiO_5 ceramics, the stress–strain curves from constant strain-rate experiments (Fig. 3b) in all cases show sustained plasticity, and strains over 15% were reached in all cases. Investigation of the microstructure of deformed specimens showed that limited

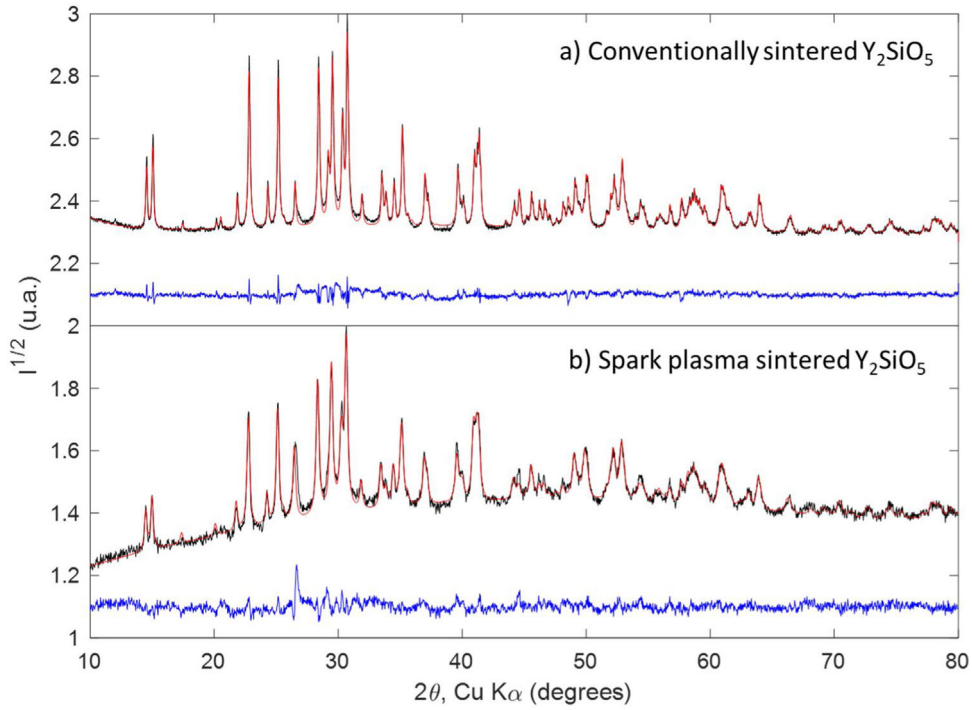

Fig. 2 – XRD patterns (black lines), result of the Rietveld refinement (red lines) and residual (blue lines) of (a) conventionally sintered and (b) spark plasma sintered Y_2SiO_5.

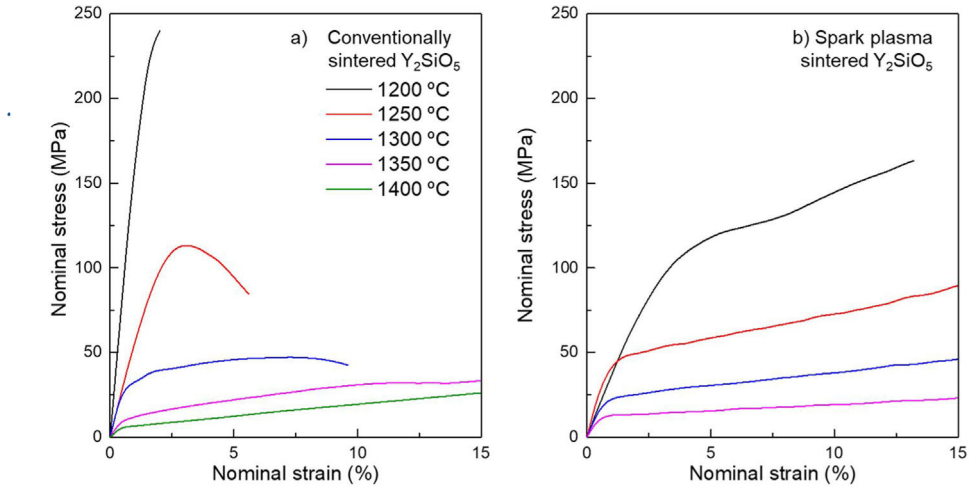

Fig. 3 – Stress–strain curves from high temperature compression tests of Y_2SiO_5 ceramics at temperatures from 1200 °C to 1350 °C.

Table 2 – Average grain size from samples tested in compression at different temperatures.

	Average grain size, $\bar{d}$ (μm)					
	Initial	1200 °C	1250 °C	1300 °C	1350 °C	1400 °C
Conventional	2.2 ± 1.2	2.5 ± 1.5	2.6 ± 1.4	2.6 ± 1.2	3.6 ± 1.8	3.6 ± 1.8
SPS	0.9 ± 0.4	0.9 ± 0.3	0.9 ± 0.3	0.9 ± 0.2	1.0 ± 0.5	

grain growth took place, in contrast with conventionally sintered Y_2SiO_5, but significant cavitation occurred (Fig. 5a). Despite this cavitation, the samples deformed homogeneously without significant cracking, and no macroscopic defects were observed. Fig. 5b shows a photograph of a sample tested up to strain of $\varepsilon \sim 20\%$ at 1350 °C (right) and an untested specimen for comparison (left). Fig. 5c shows micrographs from a SPS sample tested at 1350 °C up to 20% strain: although cavitation is evident in the first panel, the higher resolution panels show that the deformed microstructure is free from dislocations.

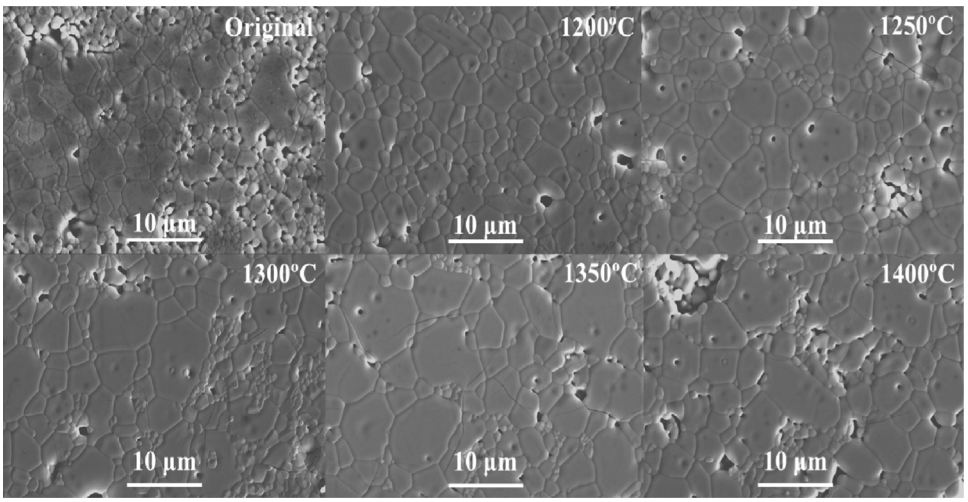

Fig. 4 – SEM micrographs of conventionally sintered Y_2SiO_5 ceramics after testing at temperatures from 1200 °C to 1400 °C, and comparison with the original as-fabricated microstructure. An increase in grain size is observed (quantitative measurements shown in Table 2).

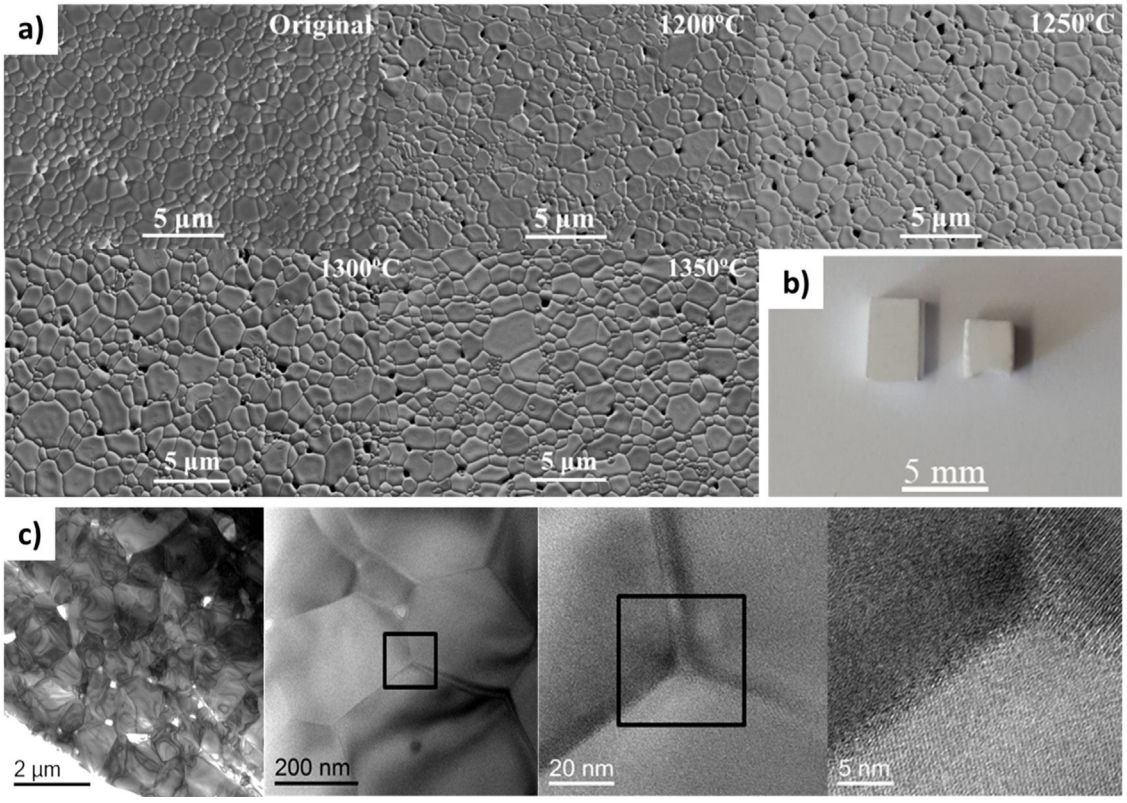

Fig. 5 – (a) SEM micrographs of SPS sintered Y_2SiO_5 ceramics after testing at temperatures from 1200 °C to 1350 °C, and comparison with the as-fabricated microstructure. No grain size growth is observed, however significant cavitation is present in the deformed specimens. (b) Photograph of a sample deformed up to a strain of $\varepsilon \sim 20\%$ at 1350 °C (right) and comparison with an undeformed, similar specimen (left). c) TEM micrographs from a sample tested up to $\varepsilon \sim 20\%$ strain at 1350 °C, where cavitation is made evident with the appearance of voids. Despite the high final strain, the microstructure appears free of dislocations.

Creep tests

In a typical creep experiment the strain is monitored as a function of time for a fixed applied stress and temperature. After a transient, deformation reaches a steady-state characterized by a constant strain rate, $\dot{\varepsilon}$. In this regime, often called secondary or stage-II creep, the strain depends on the applied load σ and the temperature T according to the Mukherjee–Dorn–Bird equation [29]

$$\dot{\varepsilon} = \frac{AD_0Gb}{kT}\left(\frac{b}{d}\right)^p\left(\frac{\sigma}{G}\right)^n e^{-Q/RT} \quad (2)$$

where n is the stress exponent, Q is the activation energy for creep, p is the grain size exponent and $R = 3.314\,J\,K^{-1}\,mol^{-1}$ is the ideal gas constant. The rest of parameters are characteristics of the material such as the shear modulus G, or its microstructure, such as the grain size d or Burger's vector modulus b.

If any grain growth is taking place during the tests, then a real steady state will not be reached since an increase in grain size will lead to a reduction in strain rate according to Eq. (2). As shown in the previous section, significant grain growth was observed during the constant strain-rate experiments for the conventionally sintered ceramic, making direct application of Eq. (2) difficult. To overcome this difficulty, a differential method was employed for the determination of the stress exponent and the activation energy. In this approach, either the stress or the temperature is kept constant during each experiment while the other is varied stepwise, and the instantaneous strain rate is measured before and after each step. Then, for an experiment where the temperature is fixed, the stress exponent can be calculated as:

$$n = \left.\frac{\partial \ln \dot{\varepsilon}}{\partial \ln \sigma}\right|_{T,d} \approx \frac{\ln \dot{\varepsilon}_2 - \ln \dot{\varepsilon}_1}{\ln \sigma_2 - \ln \sigma_1} \quad (3)$$

where $\dot{\varepsilon}_1, \sigma_1$ and $\dot{\varepsilon}_2, \sigma_2$ are the strain rate and applied stress before and after the change in load, respectively. Similarly, for a constant stress experiment where the temperature is changed step-wise, the activation energy for creep can be calculated as:

$$n = \left.\frac{\partial \ln \dot{\varepsilon}}{\partial (1/T)}\right|_{\sigma,d} \approx -R\frac{\ln \dot{\varepsilon}_2 - \ln \dot{\varepsilon}_1}{1/T_2 - 1/T_1} \quad (4)$$

Fig. 6 shows the results of the creep experiments, where $\ln \dot{\varepsilon}$ is plotted vs the total strain ε. In all plots a true steady state is not reached. This can be due to two reasons: first, the tests were performed at a constant applied load which means that the actual stress is decreasing as deformation proceeds, since a continuous increase in the transverse section due to deformation results in a decrease in stress. Second, concurrent grain growth during tests can result in a continuous decrease in strain rate. Importantly, Fig. 6 shows that the studied ceramics can sustain deformations up to 60% in compression at 1300 °C without macroscopic damage.

Table 3 shows the calculated stress exponents and activation energies for both ceramics, as calculated from the creep curves of Fig. 6.

Table 3 – Stress exponent n and activation energy for creep Q determined from constant load creep experiments.

	Stress exponent n	Activation energy Q ($kJ\,mol^{-1}$)
Conventionally sintered	1.0 ± 0.3	480 ± 60
Spark-plasma sintered	2.4 ± 0.4	520 ± 80

The marked difference in stress exponent between the two ceramics is another indication that the two Y_2SiO_5 deform plastically via different mechanisms. A stress exponent $n \sim 1$ is normally indicative of diffusional creep, either through the bulk or the grain boundaries, whereas a stress exponent of $n \sim 2$ is normally found in superplastic ceramics and attributed to a grain boundary sliding deformation mechanism accommodated by diffusion [30].

The activation energies are similar for both ceramics when the standard deviation is considered, indicating that although the deformation mechanisms differ, the accommodation mechanism is similar and that the rate-controlling species for diffusion could be the same. Calculations performed by Liu et al. [31] showed that that oxygen vacancy is the predominant vacancy species in Y_2SiO_5 and calculated an activation energy of oxygen self-diffusion of 430–480 $kJ\,mol^{-1}$, which is in the range of our measured values, allowing us to conclude that creep is accommodated by bulk self-diffusion and controlled by oxygen vacancies.

Despite the small differences in grain size, our results show that the two ceramics deform by different mechanisms, evidenced by the transition from a stress exponent $n = 2$ to $n = 1$ when the initial grain size changes from ~0.9 μm to ~2.4 μm. The transition to a stress exponent of $n = 2$ when the grain size decreases below about 1 μm has been reported for yttria stabilized zirconia with grain sizes ranging from 0.3 to 17 μm [32] although there is still no simple explanation for this effect. A similar transition has been shown in the case of $La_{9.33}Si_6O_{26}$ ceramics processed by conventional sintering ($d = 1.1$ μm, $n = 1$) and SPS ($d = 0.2$ μm, $n = 2$) [28].

It has been shown that due to the rapid heating and cooling, SPS can lead to the apparition of residual stress or result in metastable microstructures that can affect the room temperature properties of the resulting ceramic. One paper found differences in the wear behavior of SiC nanoceramics processed by SPS after a gentle annealing at 1200 °C for 12 h in vacuum [33], while another reported large differences in both room-temperature bending strength and creep for SPS alumina polycrystals after annealing for 5 h in air at 1000 °C [34]. Both papers attribute this difference to the presence of residual stresses in the as-processed samples that are relaxed after annealing. In our case, and due to the high temperatures employed, the slow heating rates and 1 h of dwell time before the start of each test should be enough to relieve any residual stress in the samples. If residual stresses are accommodated by mass transport and ultimately diffusion, for our determined activation energy of ~500 kJ and assuming an Arrhenius-type behavior, a 1 h annealing at 1300 °C is equivalent to ~12 h at 1200 °C, the SPS peak temperature and thus any residual stresses will have relaxed before the start of each test.

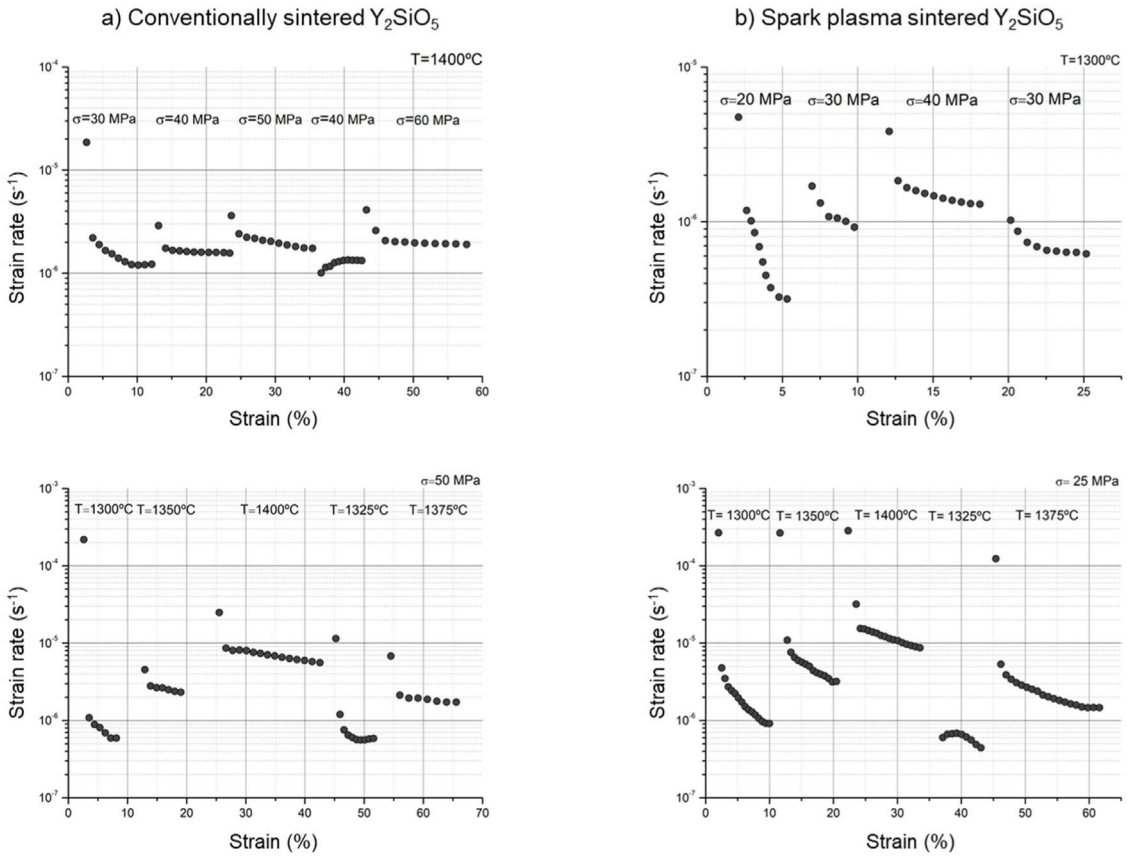

Fig. 6 – Strain rate vs. strain curves for: (a) conventionally sintered Y_2SiO_5 in constant temperature (top) and constant stress (bottom) tests, (b) spark-plasma sintered Y_2SiO_5 in constant temperature (top) and constant stress (bottom) tests.

Conclusions

Close to fully dense Y_2SiO_5 polycrystals were prepared by two different synthesis and sintering methods, to obtain ceramics suitable for high-temperature compression experiments. In the case of conventionally sintered ceramics, densities of ~92% were achieved with a mean grain size of 2.2 μm, whereas spark-plasma sintered ceramics showed a density of ~95% and a mean grain size of 0.9 μm. Despite the small differences in microstructure, both ceramics showed markedly different mechanical properties. The conventionally sintered ceramic exhibited a brittle to ductile transition at ~1250 °C as deformation mechanisms became active to accommodate deformation, whereas the finer-grained ceramic showed extensive deformation and close to superplastic behavior in the whole temperature range studied. Microstructural investigation showed cavitation in the spark-plasma sintered ceramic without grain coarsening, while the conventionally sintered ceramic showed appreciable grain growth. Creep experiments confirmed the difference between the two microstructures: the larger-grained ceramic showed a stress exponent of $n \sim 1$ indicative of diffusional creep while the finer-grained ceramic exhibited a stress exponent of $n \sim 2.5$, compatible with grain boundary sliding. Activation energy was similar in both cases and compatible with that previously reported for oxygen self-diffusion.

Acknowledgements

R. Cabezas-Rodriguez acknowledges a travel grant from the University of Seville (PP2015-4234) to École CentraleSupélec (France). X-ray diffraction and electron microscopy was performed at the CITIUS central services of the University of Seville (Spain). We are thankful to B. Lacroix for his help with TEM imaging.

The authors thank Prof. Víctor M. Orera, to whose memory this work is dedicated, for his many contributions to the field and for always being a source of inspiration.

REFERENCES

[1] K.N. Lee, R.A. Miller, Oxidation behavior of mullite-coated SiC and SiC/SiC composites under thermal cycling between room temperature and 1200–1400 °C, J. Am. Ceram. Soc. 79 (1996) 620–626, http://dx.doi.org/10.1111/j.1151-2916.1996.tb07920.x.

[2] I. Spitsberg, J. Steibel, Thermal and environmental barrier coatings for SiC/SiC CMCs in aircraft engine applications, Int. J. Appl. Ceram. Technol. 1 (2004) 291–301, http://dx.doi.org/10.1111/j.1744-7402.2004.tb00181.x.

[3] N.S. Jacobson, Corrosion of silicon-based ceramics in combustion environments, J. Am. Ceram. Soc. 76 (1993) 3–28, http://dx.doi.org/10.1111/j.1151-2916.1993.tb03684.x.

[4] R.C. Robinson, J.L. Smialek, SiC recession caused by SiO_2 scale volatility under combustion conditions: I. Experimental results and empirical model, J. Am. Ceram. Soc. 82 (1999) 1817–1825, http://dx.doi.org/10.1111/j.1151-2916.1999.tb02004.x.
[5] E.J. Opila, J.L. Smialek, R.C. Robinson, D.S. Fox, N.S. Jacobson, SiC recession caused by SiO_2 scale volatility under combustion conditions: II. Thermodynamics and gaseous-diffusion model, J. Am. Ceram. Soc. 82 (1999) 1826–1834, http://dx.doi.org/10.1111/j.1151-2916.1999.tb02005.x.
[6] J.L. Smialek, R.C. Robinson, E.J. Opila, D.S. Fox, N.S. Jacobson, SiC and Si_3N_4 recession due to SiO_2 scale volatility under combustor conditions, Adv. Compos. Mater. 8 (1999) 33–45, http://dx.doi.org/10.1163/156855199X00056.
[7] K.N. Lee, Current status of environmental barrier coatings for Si-based ceramics, Surf. Coatings Technol. 133–134 (2000) 1–7, http://dx.doi.org/10.1016/S0257-8972(00)00889-6.
[8] K.N. Lee, D.S. Fox, N.P. Bansal, Rare earth silicate environmental barrier coatings for SiC/SiC composites and Si_3N_4 ceramics, J. Eur. Ceram. Soc. 25 (2005) 1705–1715, http://dx.doi.org/10.1016/j.jeurceramsoc.2004.12.013.
[9] H.J. Seifert, S. Wagner, O. Fabrichnaya, H.L. Lukas, F. Aldinger, T. Ullmann, M. Schmücker, H. Schneider, Yttrium silicate coatings on chemical vapor deposition-SiC-precoated C/C-SiC: thermodynamic assessment and high-temperature investigation, J. Am. Ceram. Soc. 88 (2005) 424–430, http://dx.doi.org/10.1111/j.1551-2916.2005.00077.x.
[10] J.D. Webster, M.E. Westwood, F.H. Hayes, R.J. Day, R. Taylor, A. Duran, M. Aparicio, K. Rebstock, W.D. Vogel, Oxidation protection coatings for C/SiC based on yttrium silicate, J. Eur. Ceram. Soc. 18 (1998) 2345–2350, http://dx.doi.org/10.1016/S0955-2219(98)00241-6.
[11] H. Jian-Feng, L. He-Jun, Z. Xie-Rong, L. Ke-Zhi, X. Xin-Bo, H. Min, Z. Xiu-Lian, L. Ying-Lou, A new SiC/yttrium silicate/glass multi-layer oxidation protective coating for carbon/carbon composites, Carbon N. Y. 42 (2004) 2356–2359, http://dx.doi.org/10.1016/j.carbon.2004.05.005.
[12] J.I. Federer, Alumina base coatings for protection of SiC ceramics, J. Mater. Eng. 12 (1990) 141–149, http://dx.doi.org/10.1007/BF02834067.
[13] K.N. Lee, R.A. Miller, N.S. Jacobson, New generation of plasma-sprayed mullite coatings on silicon carbide, J. Am. Ceram. Soc. 78 (1995) 705–710, http://dx.doi.org/10.1111/j.1151-2916.1995.tb08236.x.
[14] K.N. Lee, D.S. Fox, J.I. Eldridge, D. Zhu, R.C. Robinson, N.P. Bansal, R.A. Miller, Upper temperature limit of environmental barrier coatings based on mullite and BSAS, J. Am. Ceram. Soc. 86 (2003) 1299–1306, http://dx.doi.org/10.1111/j.1151-2916.2003.tb03466.x.
[15] J.F. Huang, H.J. Li, X.R. Zeng, K.Z. Li, Yttrium silicate oxidation protective coating for SiC coated carbon/carbon composites, Ceram. Int. 32 (2006) 417–421, http://dx.doi.org/10.1016/j.ceramint.2005.03.018.
[16] Y. Ogura, M. Kondo, T. Morimoto, A. Notomi, T. Sekigawa, Oxygen permeability of Y_2SiO_5, Mater. Trans. 42 (2001) 1124–1130, http://dx.doi.org/10.2320/matertrans.42.1124.
[17] J. Wang, S. Tian, G. Li, F. Liao, X. Jing, Preparation and X-ray characterization of low-temperature phases of R_2SiO_5 (R = rare earth elements), Mater. Res. Bull. 36 (2001) 1855–1861, http://dx.doi.org/10.1016/S0025-5408(01)00664-X.
[18] D. Boyer, B. Derby, Yttrium silicate powders produced by the sol–gel method, structural and thermal characterization, J. Am. Ceram. Soc. 86 (2003) 1595–1597, http://dx.doi.org/10.1111/j.1151-2916.2003.tb03520.x.
[19] C. Cannas, M. Mainas, A. Musinu, G. Piccaluga, A. Speghini, M. Bettinelli, Nanocrystalline luminescent Eu^{3+}-doped Y_2SiO_5 prepared by sol–gel technique, in: Opt. Mater. (Amst.), Elsevier, 2005, pp. 1506–1510, http://dx.doi.org/10.1016/j.optmat.2005.01.008.
[20] Z. Sun, Y. Zhou, M. Li, Effect of $LiYO_2$ on the synthesis and pressureless sintering of Y_2SiO_5, J. Mater. Res. 23 (2008) 732–736, http://dx.doi.org/10.1557/jmr.2008.0085.
[21] Z. Sun, J. Wang, M. Li, Y. Zhou, Mechanical properties and damage tolerance of Y_2SiO_5, J. Eur. Ceram. Soc. 28 (2008) 2895–2901, http://dx.doi.org/10.1016/j.jeurceramsoc.2008.04.029.
[22] Z. Sun, M. Li, Y. Zhou, Thermal properties of single-phase Y_2SiO_5, J. Eur. Ceram. Soc. 29 (2009) 551–557, http://dx.doi.org/10.1016/j.jeurceramsoc.2008.07.026.
[23] Z. Sun, M. Li, Y. Zhou, Recent progress on synthesis, multi-scale structure, and properties of Y–Si–O oxides, Int. Mater. Rev. 59 (2014) 357–383, http://dx.doi.org/10.1179/1743280414Y.0000000033.
[24] N. Al Nasiri, N. Patra, D. Horlait, D.D. Jayaseelan, W.E. Lee, Thermal properties of rare-earth monosilicates for EBC on Si-based ceramic composites, J. Am. Ceram. Soc. 99 (2016) 589–596, http://dx.doi.org/10.1111/jace.13982.
[25] B.J. Harder, J.D. Almer, C.M. Weyant, K.N. Lee, K.T. Faber, Residual stress analysis of multilayer environmental barrier coatings, J. Am. Ceram. Soc. 92 (2009) 452–459, http://dx.doi.org/10.1111/j.1551-2916.2008.02888.x.
[26] B.J. Harder, J. Ramirez-Rico, J.D. Almer, K.N. Lee, K.T. Faber, Chemical and mechanical consequences of environmental barrier coating exposure to calcium-magnesium-aluminosilicate, J. Am. Ceram. Soc. 94 (2011), http://dx.doi.org/10.1111/j.1551-2916.2011.04448.x.
[27] M. Aparicio, R. Moreno, A. Durán, Colloidal stability and sintering of yttria-silica and yttria-silica-alumina aqueous suspensions, J. Eur. Ceram. Soc. 19 (1999) 1717–1724, http://dx.doi.org/10.1016/S0955-2219(98)00267-2.
[28] D. Ciria, M. Jiménez-Melendo, V. Aubin, G. Dezanneau, Creep properties of high dense $La_{9.33}Si_6O_{26}$ electrolyte for SOFCs, J. Eur. Ceram. Soc. 40 (2020) 1989–1998, http://dx.doi.org/10.1016/J.JEURCERAMSOC.202001004.
[29] A.K. Mukherjee, J.E. Bird, J.E. Dorn, Trans. Am. Soc. Metals 62 (1969) 155–179.
[30] J. Ramirez-Rico, J. Martinez-Fernandez, High-temperature mechanical behavior of hard ceramics, in: Compr. Hard Mater., Elsevier, 2014, pp. 321–343, http://dx.doi.org/10.1016/B978-0-08-096527-7.00030-1.
[31] B. Liu, J. Wang, F. Li, J. Wang, Y. Zhou, Mechanisms of mono-vacancy and oxygen permeability in Y2SiO5 orthosilicate studied by first-principles calculations, J. Am. Ceram. Soc. 95 (3) (2012) 1093–1099, http://dx.doi.org/10.1111/j.1551-2916.2011.05046.x.
[32] M. Jiménez-Melendo, A. Domínguez-Rodríguez, A. Bravo-León, Superplastic flow of fine-grained yttria-stabilized zirconia polycrystals: constitutive equation and deformation mechanisms, J. Am. Ceram. Soc. 81 (1998) 2761–2776, http://dx.doi.org/10.1111/J.1151-2916.1998.TB02695.X.
[33] A.L. Ortiz, E. Ciudad, T.N. Baymukhametov, O. Borrero-López, A.L. Vasiliev, M. Nygren, Improving the sliding wear resistance of SiC nanoceramics fabricated by spark plasma sintering via gentle post-sintering annealing, Scr. Mater. 77 (2014) 9–12, http://dx.doi.org/10.1016/J.SCRIPTAMAT.201401002.
[34] I. Álvarez-Clemares, A. Borrell, S. Agouram, R. Torrecillas, A. Fernández, Microstructure and mechanical effects of spark plasma sintering in alumina monolithic ceramics, Scr. Mater. 68 (2013) 603–606, http://dx.doi.org/10.1016/J.SCRIPTAMAT.201212016.